DE-Vol. 75, Active Control of Vibration and Noise
ASME 1994

DESIGN OF A ROTATIONAL ACTUATOR FOR GLOBAL STABILIZATION OF TRANSLATIONAL MOTION

Robert T. Bupp, Chih-Jian Wan, Vincent T. Coppola,[1] and Dennis S. Bernstein[2]
Department of Aerospace Engineering
University of Michigan
Ann Arbor, Michigan

Abstract

In this paper, we present a rotational actuator for global stabilization of a translational oscillatory system. The actuator involves a standard rotary motor with an eccentric mass attached to the shaft to couple the rotational and translational motions. We explore actuator design considerations as well as practical controller issues such as peak torque reduction, stabilization with bounded torque, and performance against single frequency sinusoidal disturbances. Two control laws are presented for this actuator: the first is based on energy considerations and actively emulates a passive absorber, while the second is the nonlinear globally asymptotically stabilizing control law obtained in [6]. Several comparisons are made between the passive absorber and the active nonlinear controller approaches.

1 INTRODUCTION

Active control techniques represent one of the most promising approaches for suppressing undesirable vibrations in a broad range of applications. The effective use of sensors, computers, and actuators in conjunction with sophisticated feedback algorithms can potentially enhance the performance of traditional passive structures.

One of the principal impediments to active vibration suppression is the development of suitable actuators for applying forces and torques to the controlled structure. Actuators based upon piezoelectric and other active materials are widely used for this purpose. To achieve higher force and stroke capability, however, high precision electromechanical devices must be used to apply forces specified by feedback control algorithms. In particular, proof-mass actuators provide single-axis control of translational motion [1, 2, 3, 4, 5]. Multiple proof-mass actuators can then be used to provide coordinated control of multi-axis motion.

One disadvantage of proof-mass actuators is the stroke limitation due to the maximum allowable proof-mass displacement. This constraint as well as other characteristics of the proof-mass actuator determine the attainable force levels as a function of frequency [5]. These saturation effects must be taken in account either by confining actuator operation to the linear regime or through nonlinear analysis.

In this paper, we investigate the construction of a force actuator for translational motion implemented by means of a standard rotary motor. By mounting an eccentric proof mass to the shaft of the motor, torque commands to the motor can be used to transmit forces to the structure. The primary advantage of such a system is that difficulties associated with stroke limitation are eliminated. However, in order to stabilize translational motion with such a device, it is necessary to account for the nonlinear interaction between the translational motion of the structure and the rotational motion of the proof mass. In the simplest case of a single-degree-of-freedom oscillator, the nonlinear interaction may be complex [7].

The problem of actively controlling such a rotational/translational proof-mass actuator was considered in [6]. In particular, nonlinear feedback control laws were obtained in [6] for globally despinning a torque-commanded oscillating eccentric rotor mounted to a single-degree-of-freedom oscillator. This work was subsequently extended to global stabilization of undamped multi-mode translational motion [13]. The control laws obtained in [6, 13] were obtained by nonlinear controller synthesis techniques [8, 9]. However, practical issues such as actuator design considerations, the effect of torque saturation, and the ability to reject persistent disturbances were not addressed in [6, 13]. The goal of the present paper, therefore, is to address these pertinent issues in the context of comparing the nonlinear control laws of [6] to an active emulation of a simple pendulum absorber.

In Section 3, we describe the design parameters associated with the development of the rotational actuator. Tradeoff plots are given to show the interdependence of the parameters and to guide actuator design.

In Section 4, we present two distinct control laws for the rotational actuator. The first control law, which is based on energy considerations, actively emulates a passive absorber. We will refer to this active implementation of the passive absorber as the "absorber control law" throughout the pa-

[1] Research supported in part by the National Science Foundation under Grant MSS-9309165.

[2] Research supported in part by the Air Force Office of Scientific Research under Grant F49620-92-J-0127.

per. Passive absorbers have been widely studied for damping translational motion, see for example [15], [14]. Our active implementation is designed so that the rotational damper can generate no more than a prescribed amount of torque to oppose the rotational velocity. As a result, the absorber control law is guaranteed to bring the system to rest without exceeding a prescribed maximum torque level. Our absorber control law involves only two design parameters, both of which can be given clear physical interpretations, thus making absorber tuning relatively intuitive.

Our absorber control law is used as a baseline comparison for the second control law, which is based on [6]. Since the nonlinear controller synthesis approach of [6] is based on the integrator backstepping methodology, we will refer to this family of control laws as the "IB" control laws. The IB control laws obtained in [6] involve six free parameters whose values can be adjusted to modify the behavior of the closed-loop system. While global asymptotic stability is assured for each allowable value of these parameters, we show that the peak applied torque level can be adjusted by choice of the parameter values.

We assess the ability of the rotational proof-mass actuator to attenuate the effect of disturbances on the closed-loop system by considering the response of the system to initial conditions as well as the response to external disturbances applied to the oscillator. Here we confine our consideration of external disturbances to the case of single-frequency disturbances of fixed amplitude. In [15], the authors develop analytical results to predict the amplitude of the steady-state limit cycle for a translational oscillator with a damped pendulum absorber subjected to a sinusoidal disturbance force. However, since our absorber control law involves a nonlinear rotational damper term, this analysis is not generally valid for our case. Furthermore, analytical results are not readily available for the IB control laws of [6]. In Section 5 we present numerical simulation results, and compare the performance of the two control laws.

The analytical and simulation results provide the basis for a Rotational/ Translational ACtuator (RTAC) Experimental Demonstration, which is currently under construction. In this paper we discuss additional implementation issues in the design of this experiment such as real-time measurements of the motor shaft angle and velocity as well as the measurements of the position and velocity of the translational oscillator.

2 DYNAMIC MODEL FOR THE TRANSLATIONAL OSCILLATOR AND ROTATIONAL ACTUATOR

The dynamical system presented in this section provides the basis for a Rotational/ Translational ACtuator (RTAC) Experimental Demonstration. This demonstration involves a torque-commanded proof-mass actuator mounted on a single-mode translational oscillator. A diagram of this arrangement, given in Figure 1, shows a cart of mass M connected by a spring of stiffness k to a wall. The rotational actuator, which is mounted on the cart, consists of a proof mass of mass m and centroidal moment of inertia I mounted a fixed distance e from its center of rotation. Control torques denoted by N are applied to the rotational proof mass, and translational disturbance forces denoted by F can be applied to the cart.

A drawing of the RTAC arrangement as it will be constructed is given in Figure 2. Toward the top of the figure is the rotary motor with incremental encoder. The motor

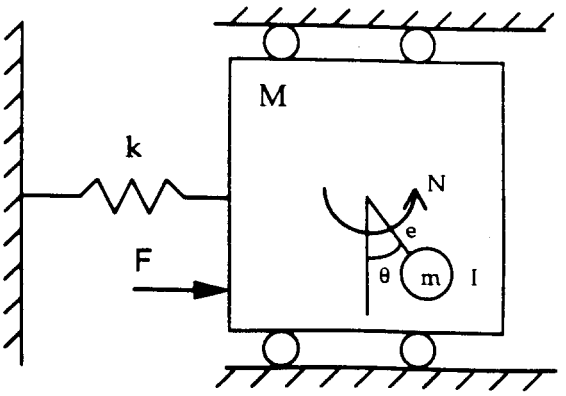

Figure 1: Translational Oscillator with Rotational Actuator

is mounted with its shaft directed downward to a platform which rides on an air rail in the horizontal plane. Affixed to the motor shaft is a steel collar, which sits inside roller bearings in the platform, and onto which the arm and eccentric mass are attached. The roller bearings transmit the inertial forces from the rotating eccentric mass to the platform.

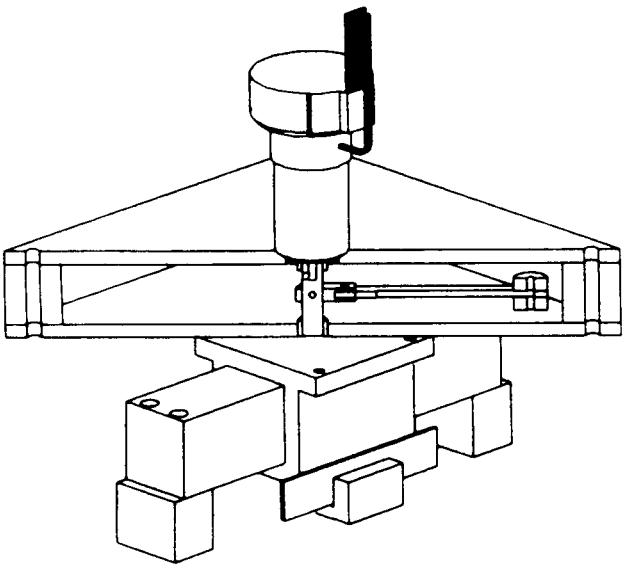

Figure 2: Hardware Implementation of the Rotational/ Translational Actuator

The overall size of the platform is roughly eight inches square, and the allowable peak-to-peak travel for the oscillator is approximately four inches. The eccentric proof mass can be fixed at any location along the arm, and it can be replaced by alternative proof masses to enrich the experimental demonstration.

The motion of the eccentric proof mass generates side forces as well as forces directed along the axis of travel. In the present arrangement, the air rail must bear these side forces as well as the torque produced by the motor. It is possible to eliminate the resulting side forces by implementing

a second RTAC whose motion mirrors the first with respect to the axis of translation, so that the side forces and torques are cancelled internally, and are not transmitted to the air rail. However, for simplicity, the experimental demonstration utilizes only one RTAC.

We will frequently refer to the portion of the system that rotates as the "actuator", or "proof mass", and to the remainder of the system as the "oscillator". Consequently, the motor shaft, the steel collar, the eccentric mass, and the arm collectively comprise the actuator, and it is their combined mass, rotary inertia, and eccentricity properties that are given by m, I, and e respectively. The nonrotating moving parts, including the platform, the various bearings and screws, the moving portion of the air slide, and the nonrotating portions of the motor, comprise the oscillator so that the total mass of these parts is given by M. The spring that provides the restoring force for the oscillator is not shown.

The equations of motion are given in [6] and are included here for completeness. Let q denote the translational position of the oscillator from its equilibrium position, and let θ denote the counter-clockwise rotational angle of the unbalanced mass, where $\theta = 0$ is perpendicular to the direction of translation, as shown in Figure 1. The equations of motion are given by

$$(M+m)\ddot{q} + kq = F - me(\ddot{\theta}\cos\theta - \dot{\theta}^2\sin\theta), \quad (1)$$

$$(I+me^2)\ddot{\theta} = N - me\ddot{q}\cos\theta. \quad (2)$$

It is convenient to normalize these equations with the substitutions

$$\xi \triangleq \sqrt{\frac{M+m}{I+me^2}}q, \qquad \epsilon \triangleq \frac{me}{\sqrt{(I+me^2)(M+m)}},$$

$$u \triangleq \frac{M+m}{k(I+me^2)}N, \qquad F_d \triangleq \frac{1}{k}\sqrt{\frac{M+m}{I+me^2}}F,$$

$$\tau \triangleq \sqrt{\frac{k}{M+m}}t.$$

With these normalizations, (1), (2) become

$$\ddot{\xi} + \xi = \epsilon(\dot{\theta}^2\sin\theta - \ddot{\theta}\cos\theta) + F_d, \quad (3)$$

$$\ddot{\theta} = -\epsilon\ddot{\xi}\cos\theta + u, \quad (4)$$

where the time derivatives denoted by superscript dot are now taken with respect to τ.

Letting $x = [x_1, x_2, x_3, x_4]^{\mathrm{T}} = [\xi, \dot{\xi}, \theta, \dot{\theta}]^{\mathrm{T}}$, the nondimensional equations of motion in first-order form are given by

$$\dot{x} = f(x) + g(x)u + d(x)F_d, \quad (5)$$

where

$$f(x) = \begin{bmatrix} x_2 \\ \left(-x_1 + \epsilon x_4^2\sin x_3\right)/\left(1-\epsilon^2\cos^2 x_3\right) \\ x_4 \\ \epsilon\cos x_3\left(x_1 - \epsilon x_4^2\sin x_3\right)/\left(1-\epsilon^2\cos^2 x_3\right) \end{bmatrix} \quad (6)$$

$$g(x) = \frac{1}{1-\epsilon^2\cos^2 x_3}\begin{bmatrix} 0 \\ -\epsilon\cos x_3 \\ 0 \\ 1 \end{bmatrix}, \quad (7)$$

$$d(x) = \frac{1}{1-\epsilon^2\cos^2 x_3}\begin{bmatrix} 0 \\ 1 \\ 0 \\ -\epsilon\cos x_3 \end{bmatrix}. \quad (8)$$

Note that the denominator $1-\epsilon^2\cos^2 x_3$ is always positive, since by definition $\epsilon < 1$. With $u = 0$ and $F_d = 0$, the equilibria of this system are found to be of the form $x = [0, 0, x_3, 0]^{\mathrm{T}}$, where x_3 denotes an arbitrary angular position of the eccentric proof mass.

3 ACTUATOR DESIGN CONSIDERATIONS

In equations (3), (4) the parameter ϵ represents the coupling between the translational and rotational motions. Since our goal is to design a rotational actuator for suppressing translational motion, the choice of this parameter is of utmost importance. Generally large values of ϵ are desired, so that the rotational actuator will have a significant effect on the translational motion.

The parameter ϵ is a function of the physical parameters m, M, I, and e. In this section, we investigate the relationship between these physical parameters and the resulting value of ϵ. For convenience, define the dimensionless variables

$$\hat{m} \triangleq m/M,$$

$$\hat{e} \triangleq e\sqrt{M/I},$$

where $\hat{m}$ is the ratio of the proof mass to the mass of the oscillator. With these variables, ϵ can be written as

$$\epsilon = \frac{\hat{m}\hat{e}}{\sqrt{(1+\hat{m}\hat{e}^2)(1+\hat{m})}}. \quad (9)$$

Using (9), tradeoff plots can be constructed to illustrate the limitations to achieving large values of ϵ. Figure 3 shows such a tradeoff plot for ϵ versus $\hat{e}$, where $\hat{m}$ is used as a parameter. Figure 3 illustrates the benefit of large values of $\hat{e}$ in increasing the coupling parameter ϵ. For fixed values of M, the value of $\hat{e}$ can be increased either by increasing the eccentricity e, or by reducing the centroidal moment of inertia I of the proof mass. This figure also shows a large actuator-to-oscillator mass ratio $\hat{m}$ may be required in order to achieve high coupling between the rotational and translational motions. When the actuator mass must be kept small relative to the oscillator mass, the coupling parameter ϵ necessarily decreases. For example, mass ratios under one percent cannot produce values of ϵ in excess of 0.1 regardless of the eccentricity of the proof mass.

4 CONTROL LAW DESIGNS

In this section, we present two control laws that stabilize the translational and rotational motions. The first control law emulates a passive absorber, with a prescribed maximum torque. The second control law, which is given in [6], is synthesized using nonlinear controller synthesis techniques. Both controllers are guaranteed to bring the rotational and translational motions to rest asymptotically from every initial condition.

4.1 Passive Absorber Controller

Consider the system of equations (1), (2) with $F = 0$. Let N_{max} denote the maximum allowable control torque magnitude. Then the control law given by

$$N = -(N_{max} - K_s)\tanh(\gamma\dot{\theta}) - K_s \sin\theta, \qquad (10)$$

with

$$N_{max} > K_s > 0, \qquad \gamma > 0, \qquad (11)$$

brings the system to rest from every initial condition, with

$$|N| \leq N_{max}. \qquad (12)$$

Note that equation (12) follows from (10) and the triangle inequality.

With the control law (10), the system (1), (2) has two distinct equilibria. They correspond to the oscillator motionless at zero translational position (no stretch in the spring), and the proof mass motionless and perpendicular to the axis of translation. The equilibrium position which includes $\theta = 0$ is stable, while the equilibrium position which includes $\theta = \pi$ is unstable. Using LaSalle's Theorem [16], it can be shown that every trajectory approaches one of these equilibria asymptotically.

The first term in the control law (10) represents a bounded torque rotational damper that always opposes the rotational motion. Thus whenever the actuator is moving, energy is dissipated from the system. The parameter γ serves as a gain for the rotational damper. Although this first term alone will bring the rotational motion to rest, simulations confirm that such a control law generally causes the eccentric mass to come to rest at $\theta = \frac{\pi}{2}$ or $\frac{3\pi}{2}$. Since at this location the translational motion does not excite the rotational motion, the translational motion need not come to rest. Thus a second term is needed to prevent the eccentric proof mass from coming to rest in this configuration.

The second term in the control law represents a nonlinear spring, which serves to pull the eccentric mass to one side using bounded torque for all values of θ. Physically, this term emulates a gravitational field whose strength is set by the parameter K_s. Thus the control law (10) has the effect of emulating a damped pendulum hanging from a translational (horizontal) oscillator.

4.2 Integrator Backstepping Controller

The controller synthesis of [6] globally asymptotically stabilizes the system (5) to the origin, provided $F_d = 0$. The control laws in [6] were obtained by using the following change of coordinates, which effect partial feedback linearization:

$$\begin{aligned} z_1(x) &\triangleq x_1 + \epsilon \sin x_3, \\ z_2(x) &\triangleq x_2 + \epsilon x_4 \cos x_3, \\ y_1(x) &\triangleq x_3, \\ y_2(x) &\triangleq x_4. \end{aligned}$$

Equation (5) can now be rewritten in terms of the new variables (z_1, z_2, y_1, y_2) as

$$\begin{aligned} \dot{z}_1 &= z_2, & (13)\\ \dot{z}_2 &= -z_1 + \epsilon \sin y_1, & (14)\\ \dot{y}_1 &= y_2, & (15)\\ \dot{y}_2 &= v, & (16) \end{aligned}$$

where

$$v = \frac{\epsilon \cos y_1}{1 - \epsilon^2 \cos^2 y_1}(z_1 - (1+y_2^2)\epsilon \sin y_1) + \frac{1}{1 - \epsilon^2 \cos^2 y_1} u \qquad (17)$$

Since (13) - (16) is in cascade form [8], the integrator backstepping procedure [9, 11] can be used to develop a globally asymptotically stabilizing control law for the variable v. The nonlinear feedback control law derived in [6] is given by

$$\begin{aligned} v = & -c_2 \left(y_2 + c_1(y_1 + c_0 \arctan z_2) + \frac{c_0(-z_1 + \epsilon \sin y_1)}{1 + z_2^2} \right) \\ & - c_2 \frac{\epsilon p_0 z_2 (\sin y_1 + \sin(c_0 \arctan z_2))}{p_1(y_1 + c_0 \arctan z_2)} + \frac{c_0 z_2}{1 + z_2^2} \\ & + (-z_1 + \epsilon \sin y_1) \left(-\frac{c_0 c_1}{1 + z_2^2} + 2\frac{c_0 z_2(-z_1 + \epsilon \sin y_1)}{(1 + z_2^2)^2} \right) \\ & - (-z_1 + \epsilon \sin y_1) \frac{\epsilon p_0 (\sin y_1 + \sin(c_0 \arctan z_2))}{p_1(y_1 + c_0 \arctan z_2)} \\ & - (-z_1 + \epsilon \sin y_1) \frac{\epsilon p_0 c_0 z_2 \cos(c_0 \arctan z_2)}{p_1 \left(1 + z_2^2\right)(y_1 + c_0 \arctan z_2)} \\ & - c_1 y_2 - \frac{\epsilon c_0 y_2 \cos y_1}{1 + z_2^2} - \frac{\epsilon p_0 z_2 y_2 \cos y_1}{p_1(y_1 + c_0 \arctan z_2)} \\ & + \frac{\epsilon p_0 z_2 y_2 (\sin y_1 + \sin(c_0 \arctan z_2))}{p_1(y_1 + c_0 \arctan z_2)^2} \\ & - \frac{p_1}{p_2}(y_1 + c_0 \arctan z_2), \end{aligned}$$

where the parameters p_0, p_1, p_2, c_0, c_1, and c_2 are all positive, and $0 < c_0 < 2$. The transformation (17) can now be used to determine the control law in terms of the normalized torque u.

While the global asymptotic stability property holds for every allowable choice of these parameters, there is no a priori bound on the torque level that will be generated by the control law for arbitrary initial conditions. However, if we are interested in a certain set of initial conditions, we can adjust the parameters in the control law to modify the required amount of torque. This is illustrated in the simulations that follow.

5 NUMERICAL SIMULATIONS

This section presents numerical simulation results for the two control laws designed in Section 4. State trajectories and required control torques are examined for both free and forced responses. The physical parameters used for simulation are $M = 9$ kg, $m = 1$ kg, $k = 10$ N/m, $I = 0.09$ kg-m^2, and $e = 0.1$. For this choice of parameters, it follows that $\epsilon = 0.1$. Note that this choice of parameters does not reflect the actual design values incorporated in the RTAC Experimental Demonstration, as these values were not available at the time this paper was written.

5.1 Free Response

Consider (5) with $F_d = 0$ and $x_0 = [0.1, 0, 0, 0]^T$. The resulting free response for the absorber controller with $T_{max} = 1$, $K_m = 0.1$, $\gamma = 0.015$ is given in Figure 4. This figure contains, at the top, a plot of the time history of the translational displacement x_1 of the oscillator. The middle plot shows the time history of the rotational displacement of the proof-mass actuator, and the bottom plot shows the time history of the torque which is generated by the motor.

To generate a comparison plot for the integrator backstepping (IB) control law, we consider three choices of control parameters. For convenience, denote the controller parameters by

$$\pi \triangleq [p_0, p_1, p_2, c_0, c_1, c_2]. \tag{18}$$

The three IB control laws, denoted $IB-1$, $IB-2$, and $IB-3$, were chosen to have control law parameters

$$\begin{aligned} \pi_1 &= [10, 0.1, 1, 1.9, 1, 1], \\ \pi_2 &= [5, 0.5, 1, 1.9, 1, 1], \\ \pi_3 &= [1, 1, 1, 1, 1, 1], \end{aligned}$$

respectively. Figure 5 shows the time history of the translational displacement x_1 of the oscillator, Figure 6 shows the time history of the rotational displacement θ of the proof-mass actuator, and Figure 7 shows the time history of the torque generated by the motor. In figures 5, 6, 7, the response curves corresponding to $IB-1$, $IB-2$, $IB-3$ are represented by solid, dashed, and dash-dot lines respectively.

Figure 5 shows that the $IB-1$ control law exibits much better settling performance compared to the absorber in Figure 4. The performance in either case depends greatly on the choice of control parameters; however, both the $IB-1$ control law and the absorber control law represent the best settling performance achieved by trial-and-error tuning. The performance of the $IB-1$ control law comes at the expense of much higher torque values, as can be seen by comparing Figure 4 and Figure 7. The required torque can be reduced by choice of control parameters, as exemplified by the $IB-3$ controller. This IB controller exhibits approximately the same amount of peak torque as the absorber controller, and the time histories for the translational displacement of the oscillator for control law $IB-3$ in Figure 5 and for the absorber control law in Figure 4 are correspondingly similar.

In this comparison, it is shown that the performance of the best absorber controller achieved by trial and error tuning can be significantly improved by the active Integrator Backstepping controllers, in particular by the $IB-1$ controller, at the expense of increased torque magnitude. It is also shown that by appropriate choice of the IB controller parameters, e.g., π_3, the required torque can be reduced, resulting in settling performance similar to the absorber control law. While this comparison is by no means exhaustive, it indicates that significant improvement in the settling time performance can be achieved by the active IB controllers as compared to the passive absorber.

5.2 Forced Response

The performance of the absorber control law and the $IB-1$ control law are now examined when the system is forced by

$$F = \sin 2t \tag{19}$$

This forcing function was chosen to give a steady-state translational displacement amplitude of the uncontrolled system of approximately 0.1 m, which corresponds to the size of the initial condition used in subsection 5.1. It should be emphasized that no further adjustments to the control parameters are made here. The absorber and the $IB-1$ control laws retain the values for the control parameters given in subsection 5.1, where they were chosen for their free response characteristics.

The time histories of the translational position of the oscillator for the absorber and $IB-1$ control laws are given in Figures 8 and 9 respectively. These figures illustrate slightly superior performance by the absorber controller – the absorber reduces the steady-state amplitude by approximately 56 percent, whereas the $IB-1$ control law reduces the steady-state amplitude by approximately 44 percent.

The time histories of the control torques for the absorber and $IB-1$ control laws are given in Figures 10 and 11 respectively. The absorber control law requires significantly lower torque to suppress the forced oscillations as compared to the $IB-1$ control law. Plots of the time histories of the eccentric proof mass in Figures 12 and 13 show that the absorber control law also requires much less movement of the proof mass than does the $IB-1$ controller. This comparison of the forced response of the absorber control law and the $IB-1$ control law suggests that comparable response to sinusoidal disturbances may be achieved by the IB controller as compared to the absorber controller. However, it also suggests that the IB controller is much less efficient at rejecting such disturbances, in that it requires an order of magnitude more torque to do so. While this comparison is by no means exhaustive, its implications are not surprising. The IB control laws achieve better settling times in the free response by adding and dissipating energy in a complicated manner. However, when subjected to persistent sinusoidal disturbances, the IB control laws retain this pattern of adding and dissipating energy, while the absorber control law is strictly dissipative. One result is a greater control stroke for the IB controller as compared to the absorber, which is beneficial for the free response performance. However, it is apparent that this complicated pattern of adding and dissipating energy does not provide efficient use of control torque in suppressing persistent disturbances.

6 CONCLUSIONS

We have presented a rotational actuator for controlling the motion of a translational oscillator. Further, we have presented two very different control laws that globally bring the rotational/translational system to rest.

The results present an interesting comparison between the passive absorber and the active nonlinear regulator approaches. To begin with, the active nonlinear regulators, represented by the IB controllers, require knowlege of the entire state vector, while the absorber controller requires only the rotational states θ and $\dot{\theta}$. Furthermore the IB feedback control laws are significantly more complicated mathematically than the absorber control laws.

Tuning the absorber control law proves to be a simpler task compared to tuning of the IB control laws. The absorber control laws have two tuning parameters, one representing the gain on the limited rotational damper and the other representing the strength of the effective gravitational

field. In contrast, the IB control laws have six tuning parameters which do not have clear physical interpretations. In the IB control law development, these parameters appear as constants in Lyapunov functions and Lyapunov function derivatives. Since the Lyapunov functions do not have clear physical interpretation, the role of these parameters is difficult to assess analytically.

The numerical simulation results provide a basis for performance comparison between these two methods of controller synthesis. These results indicate that the IB control laws may offer significantly better settling time performance in response to initial conditions, as compared to the absorber control laws. The results presented indicate that the best IB control law settles in less than half the time required for the absorber. The results for the forced response comparison show that the two methods exhibit similar steady-state limit cycles, although the absorber control law utilizes significantly less torque in the process. However, it should be noted that the IB control laws were originally designed to achieve global asymptotic stability, and not to suppress persistent disturbances.

These comparative results are preliminary. It is yet to be shown how the two control laws would compare for significantly larger or smaller initial conditions, or for different amplitudes and frequencies of the disturbances. Further numerical as well as experimental results are forthcoming.

References

[1] D. C. Zimmerman, G. C. Hornor, and D. J. Inman, "Microprocessor Controlled Force Actuator," *J. Guid. Contr. Dyn.*, Vol. 11, pp. 230-236, 1988.

[2] H. Politansky and W. D. Pilkey, "Suboptimal Feedback Vibration Control of a Proof-Mass Actuator," *J. Guid. Contr. Dyn.*, Vol. 12, pp. 691-697, 1989.

[3] F. Ham, S. Greeley, and B. Henniges, "Active Vibration Suppression for the Mast Flight System," *IEEE Contr. Sys. Mag.*, Vol. 9, No. 1, pp.85-90, 1989.

[4] D. J. Phillips, D. C. Hyland, and E. G. Collins, Jr., "Experimental Demonstration of Active Vibration Control for Flexible Structures," *Proc. Conf. Dec. Contr.*, pp. 2024-2029, 1990.

[5] D. K. Lindner, T. P. Celano, E. N. Ide, "Vibration Suppression Using a Proofmass Actuator Operating in Stroke/Force Saturation," *J. Vibr. Acoustics*, Vol 113, pp. 423-433, 1991.

[6] C. -J. Wan, D. S. Bernstein, and V. T. Coppola, "Global Stabilization of the Oscillating Eccentric Rotor," submitted to *Int. J. Nonlinear Mechanics*.

[7] R. M. Evan-Iwanowski, *Resonance Oscillations in Mechanical Systems*, Elsevier, 1976.

[8] E. D. Sontag and H. J. Sussman, "Further Comments on the Stabilizability of the Angular Velocity of a Rigid Body," *Sys. Contr. Lett.*, Vol. 12, pp. 213-217, 1988.

[9] I. Kanellakopoulos, P. V. Kokotovic, and A. S. Morse, "A Toolkit for Nonlinear Feedback Design," *Sys. Contr. Lett.*, Vol. 18, pp. 83-92, 1992.

[10] R. Marino, "On The Largest Feedback Linearizable Subsystems," *Sys. Contr. Lett.*, Vol. 10, pp. 201-206, 1988.

[11] P. V. Kokotovic, "The Joy of Feedback: Nonlinear and Adaptive," *IEEE Contr. Sys. Mag.*, pp. 7-17, June 1992.

[12] A. Bacciotti, *Local Stabilizability of Nonlinear Control Systems*, Series on Advances in Mathematics for Applied Sciences, Vol. 8, World Scientific, Singapore, 1992.

[13] R. Bupp, V. T. Coppola, and D. S. Bernstein, "Vibration Suppression of Multi-Modal Translational Motion Using a Rotational Actuator," to appear in *Proc. Conf. Dec. Contr.*, 1994.

[14] M. Cartmell, "An Adaptive Autoparametric Vibration Absorber," *Second Conf. on Recent Advances in Active Control of Sound and Vibration*, pp. 495-505, Blacksburg, VA, 1993.

[15] B. G. Korenov and L. M. Reznikov, *Dynamic Vibration Absorbers Theory and Technical Applications*, Wiley, 1993.

[16] H. Khalil, *Nonlinear Systems*, Macmillan, 1992.

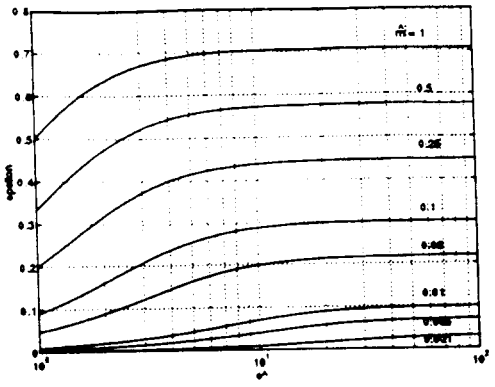

Figure 3: Tradeoff plot for ϵ versus $\hat{e}$ parameterized by $\hat{m}$

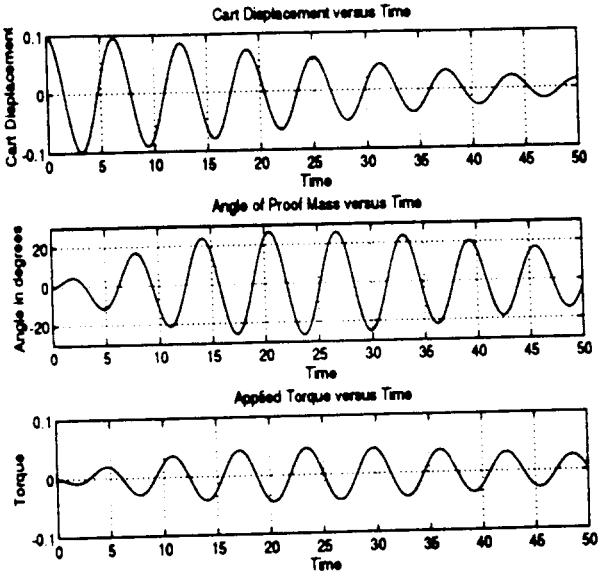

Figure 4: Initial Condition Response for the Absorber-Based Controller

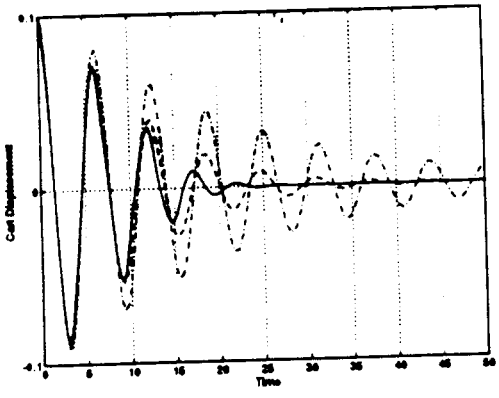

Figure 5: Time History of the Oscillator Position for Various Control Laws

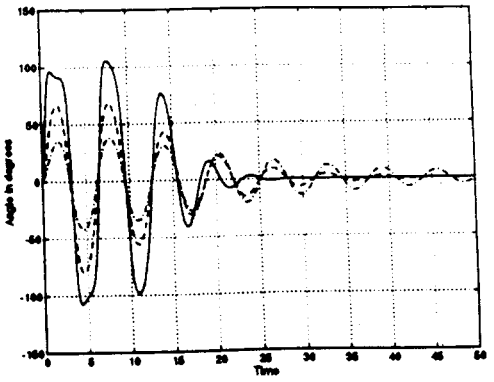

Figure 6: Time history of the Rotational Position of the Proof-Mass Actuator For Various Control Laws

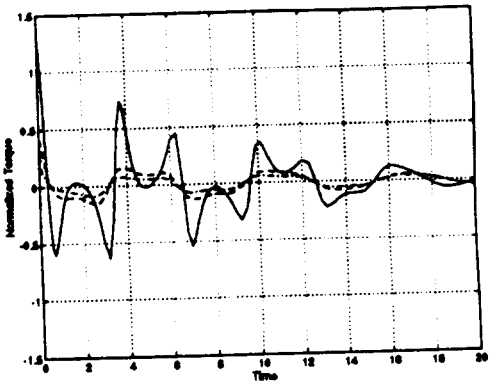

Figure 7: Time History of the Control Torque for Various Control Laws

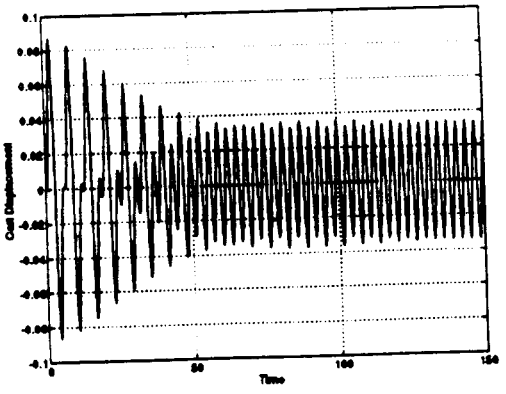

Figure 8: Time History of the Translational Position for the Absorber Control Law

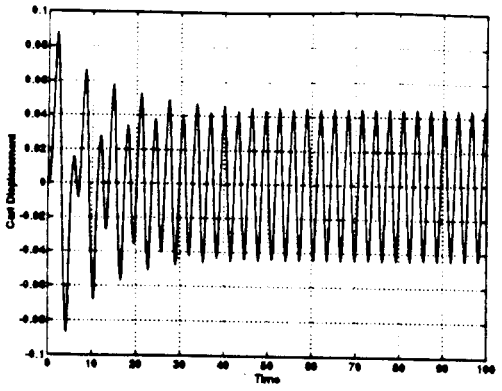

Figure 9: Time History of the Translational Position for the $IB-1$ Control Law

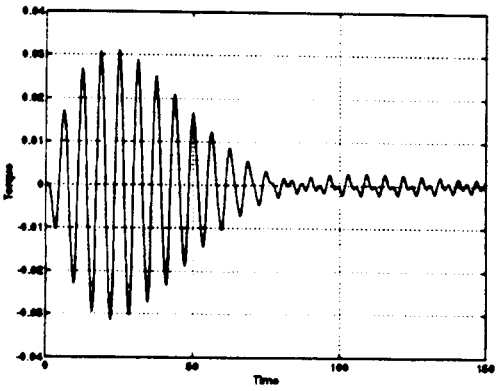

Figure 10: Time History of the Torque Required for the Absorber Controller

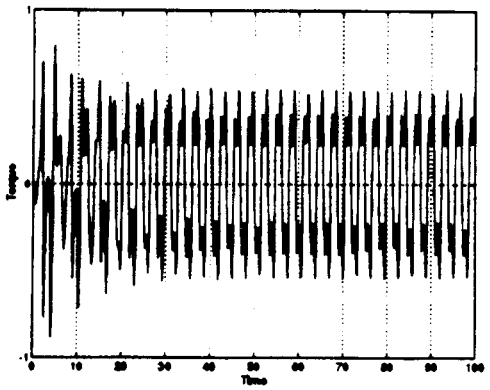

Figure 11: Time History of the Torque Required for the $IB-1$ Controller

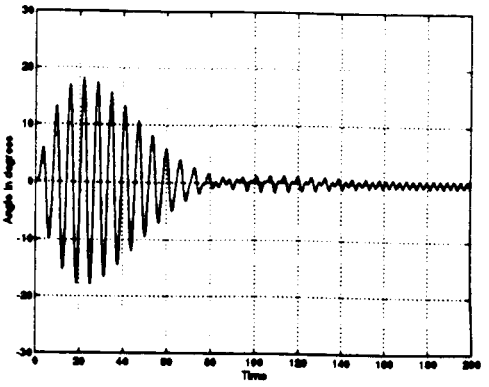

Figure 12: Time History of the Angle of the Proof Mass for the Absorber Control Law

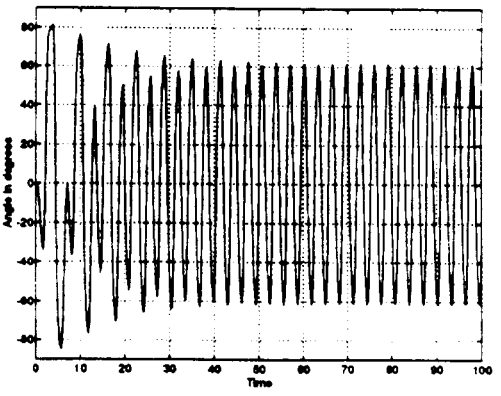

Figure 13: Time History of the Angle of the Proof Mass for the $IB-1$ Control Law